Nanoscale

Accepted Manuscript

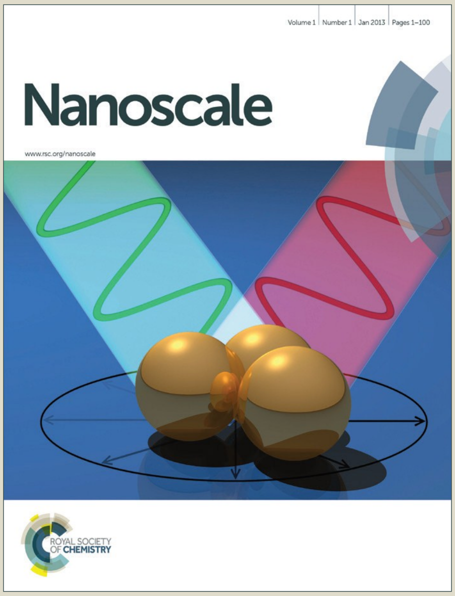

ROYAL SOCIETY OF CHEMISTRY

www.rsc.org/nanoscale

Journal Name

ARTICLE

Plasmon-Enhanced Two-Photon-Induced Isomerization for Highly-Localized Light-Based Actuation of Inorganic/Organic Interfaces

Received 00th January 20xx,
Accepted 00th January 20xx

DOI: 10.1039/x0xx00000x

www.rsc.org/

Chang-Keun Lim,[a] Xin Li,[b] Yue Li,[c] Kurt L. M. Drew,[d] J. Pablo Palafox-Hernandez,[d] Zhenghua Tang,[e] Alexander Baev,[a] Andrey N. Kuzmin,[a] Marc R. Knecht,[e] Tiffany R. Walsh,[d] Mark T. Swihart,[c] Hans Ågren[b] and Paras N. Prasad*[a,f]

Two-photon initiated photo-isomerization of an azobenzene moiety adsorbed on silver nanoparticles (Ag NPs) is demonstrated. The azobenzene is linked to a materials-binding peptide that brings it into intimate contact with the Ag NP surface, producing a dramatic enhancement of its two-photon absorbance. An integrated modeling approach, combining advanced conformational sampling with Quantum Mechanics/Capacitance Molecular Mechanics and response theory, shows that charge transfer and image charges in the Ag NP generate local fields that enhance two-photon absorption of the *cis* isomer, but not the *trans* isomer, of adsorbed molecules. Moreover, dramatic local field enhancement is expected near the localized surface plasmon resonance (LSPR) wavelength, and the LSPR band of the Ag NPs overlaps the azobenzene absorbance that triggers *cis* to *trans* switching. As a result, the Ag NPs enable two-photon initiated *cis* to *trans* isomerization, but not *trans* to *cis* isomerization. Confocal anti-Stokes fluorescence imaging shows that this effect is not due to local heating, while the quadratic dependence of switching rate on laser intensity is consistent with a two-photon process. Highly localized two-photon initiated switching could allow local manipulation near the focal point of a laser within a 3D nanoparticle assembly, which cannot be achieved using linear optical processes.

Introduction

Configurational switching of ligands on nanostructures provides a powerful mechanism for changing properties of hybrid inorganic/organic materials. Such switchable interfaces[1-4] are of particular interest in the field of bionanocombinatorics, which aims to exploit biomolecular non-covalent recognition to assemble nanoparticles (NPs) into ordered arrangements. Incorporation of a switchable interface into bionanocombinatoric assemblies could enable stimuli-responsive reconfiguration of these assemblies. Photoswitchable (PS) materials[5-7] whose structural, optical and electronic properties change reversibly upon exposure to light, have received considerable attention for applications such as high density data storage[8] and actuating devices.[9,10] Minimizing the size of such devices while providing precise control of them requires a light-addressing method with high spatial resolution. In this regard, two-photon absorption (TPA), a nonlinear optical process that can be targeted to occur only in a very small focal volume, is a very promising approach for locally switching PS materials at desired positions within three-dimensional (3D) assemblies.[11] Thus, we are interested here in combining the concept of a switchable inorganic/organic interface with TPA-driven switching.

Azobenzene, a prototypical PS molecule, changes its configuration upon linear or nonlinear excitation.[5] However, because the azobenzene parent molecule has a very low TPA cross-section, to achieve nonlinear optical switching, researchers have enhanced its nonlinear optical properties by modification with electron–donor and/or –acceptor moieties,[12,13] and by conjugation to light harvesting dendrons.[14] Another potential means of enhancing the effective TPA cross-section is to exploit metallic nanostructures that exhibit localized surface plasmon resonance (LSPR).[15-20] Such plasmonic enhancement of nonlinear optical processes like TPA is highly dependent upon the distance between the molecule and metal NP. Thus, intimate contact of the PS molecule with the NP is required.

Here, we show that by using a ligand that promotes multiple non-covalent interactions with the inorganic surface, along with a PS moiety, we can create an inorganic-organic interface that undergoes reconfiguration via two-photon initiated photoisomerization. We employ hybrid molecules, combining a peptide-based metal binding ligand with a photoswitchable

---

[a] Institute for Laser Photonics and Biophotonics, University at Buffalo (SUNY), Buffalo, NY 14260, USA. E-mail: pnprasad@buffalo.edu
[b] Division of Theoretical Chemistry and Biology, School of Biotechnology, KTH Royal Institute of Technology, SE-10691 Stockholm, Sweden.
[c] Department of Chemical and Biological Engineering, University at Buffalo (SUNY), Buffalo, NY 14260, USA.
[d] Institute for Frontier Materials, Deakin University, Geelong, 3216 VIC, Australia.
[e] Department of Chemistry, University of Miami. 1301 Memorial Drive, Coral Gables, Florida 33146, USA.
[f] Department of Chemistry, Korea University, Seoul, Korea.

†Electronic Supplementary Information (ESI) available: Additional UV-vis, thermal imaging, calculation data. See DOI: 10.1039/x0xx00000x

azobenzene moiety, as capping ligands for NP generation and stabilization, and further demonstrate that the inorganic-organic interface in these nanomaterials can be reconfigured using two-photon excitation (TPE). Specifically, to realize material-selective binding and Ag NP-enhanced two-photon isomerization, we linked a Au/Ag-binding peptide (AuBP1:WAGAKRLVLRRE)[20] to a non-electron-donor/-acceptor (non D/A) modified azobenzene at either the N- or C-terminus of the peptide. We then prepared peptide/azobenzene capped Ag NPs to study the linear and nonlinear optical isomerization behavior of the azobenzene moieties in contact with the metal surfaces. The results show that peptide/*cis*-azobenzene hybrids, when in direct contact with the Ag NP surface, are isomerized upon TPE through a selective enhancement by the Ag NPs. No two-photon switching for the reverse photoisomerization is observed for peptide/*trans*-azobenzene hybrids on Ag. We use a unique combination of advanced conformational sampling molecular dynamics simulations and response theory in the framework of the newly developed Quantum Mechanics/ Capacitance Molecular Mechanics paradigm, together with an experimental study using confocal anti-Stokes fluorescence-based thermal imaging to establish that the basis for this effect is electronic, and not thermal.

Experimental

Synthesis of (E)-4,4'-(diazene-1,2-diyl)bis(N-(2-(2,5-dioxo-2,5-dihydro-1H-pyrrol-1-yl)ethyl) benzamide) (MAM)

Azobenzene-4,4'-dicarboxylic acid (2.67 g, 9.9 mmol) and thionyl chloride (60 mL) were refluxed overnight at 85 °C. The solution was evaporated three times from toluene and the solid azobenzene-4,4'-dicarboxylic acid chloride was obtained (Yield: 98%). azobenzene-4,4'-dicarboxylic acid chloride (307 mg, 1 mmol) was dissolved in methylene chloride (10 mL) and mixed with a solution of N-(2-aminoethyl)maleimide hydrochloride (620 mg, 3.5 mmol) and TEA (0.7 mL) in methylene chloride (10 mL). The mixture was stirred overnight at room temperature and evaporated. The product was re-crystallized from ethanol to give MAM as an orange powder (Yield: 45%). ^{1}H NMR (DMSO-d_6, 500 MHz, δ): 8.76 (t, J = 6 Hz, 2H), 7.94-7.97 (m, 8H), 7.02 (s, 4H), 3.60 (t, J =5.5 Hz, 4H), 3.43(q, J = 5.5 Hz, 4H). ^{13}C NMR (DMSO-d_6, 75 MHz, δ): 171.11, 165.72, 153.21, 136.98, 134.55, 128.43, 122.51, 37.73, 37.10. HR-MS (ESI$^+$) m/z: $[M + H]^+$ calcd for $C_{26}H_{22}N_6O_6$, 514.50; Found, 514.16.

Peptide synthesis and MAM coupling

The AuBP1C and CAuBP1 peptides were synthesized using standard FMOC protocols on a TETRAS solid phase peptide synthesizer (CreoSalus). The peptide was cleaved from the resin, purified by reverse phase HPLC, and confirmed via MALDI-TOF mass spectrometry. Once the peptide was confirmed, coupling of the MAM at the incorporated cysteine residue proceeded. In a typical reaction, 27.0 mg of the peptide (either AuBP1C or CAuBP1) was dissolved in 4 mL of DMF, which was then added to a MAM solution in DMF (13.5 mg dissolved in 2 mL DMF). In this reaction, the molar ratio of MAM:peptide is 1:4, which promotes coupling of only one peptide per MAM. Once initiated, the reaction was stirred for 3 days, after which 150 mL of ethyl ether was added, resulting in precipitation of a yellow solid. Due to solubility differences, ether precipitation resulted in sample purification from unreacted MAM. The sample was centrifuged to form a pellet, the supernatant was removed, and more ethyl ether was added. This process was repeated two more times to increase the final purity of the peptide/MAM hybrid. After centrifuge purification, the sample was further purified using reverse phase HPLC and confirmed with MALDI-TOF mass spectrometry.

Silver nanoparticle synthesis

In a typical synthesis, 10 µL of a 0.1 M aqueous solution of $AgNO_3$ was diluted in 2.96 mL of water and then mixed with 2 mL of a 0.25 mM aqueous solution of AuBP1C-MAM or MAM-CAuBP1 in a vial, resulting in a Ag:MAM-peptide ratio of 2. The solution was thoroughly mixed for at least 15 min, followed by injection of 30 µL of an ice cold, freshly prepared, 0.1 mM $NaBH_4$ aqueous solution. Upon the addition of reducing agent, the color of the Ag solution changed from light yellow to bright yellow. The reaction was allowed to continue undisturbed for 1 h at room temperature to ensure complete reduction. The size and shape of the Ag nanoparticles were characterized using a JEOL JEM-2010 TEM operating at a working voltage of 200 kV. The specimen was prepared by drop-casting 15 µL of the Ag NP dispersion onto a carbon-coated Cu TEM grid. The optical absorbance spectra of Ag nanoparticles were measured using a Shimadzu UV-3101PC spectrometer employing a 1 cm quartz cuvette.

Photoswitching Experiments

Before the nanoparticle suspensions were used in switching experiments, they were purified by a Centricon filter (3000 MWCO) to remove any unbound peptides. UV-vis spectra were recorded after light irradiation using 1 cm quartz cuvettes. For the linear photoswitching of the azobenzene moiety, sample irradiation was performed with monochromatic light from a Xe lamp and monochromator. For the nonlinear photoswitching experiments, a femtosecond laser pulse (average power up to ~300 mW, 90 fs pulses at 82 MHz repetition rate), using a Ti:sapphire laser (Tsunami, Spectra-Physics) pumped by a frequency-doubled diode pumped solid-state laser (Millennia, Spectra-Physics) was focused on the middle section of the cuvette. The laser power was adjusted using a round, variable reflective ND filter (NDHN, SIGMAKOKI) and power/energy analyzer (FieldMaster™ GS, Coherent).

Confocal thermal imaging

For the thermal imaging experiment, MAM-CAuBP1 capped Ag NPs or two-photon dye AF-350 (donated by the U.S. Air Force Research Lab) was mixed with probe dye Rhodamine 101 (~80 μM) in mixture of DMSO and water (4:1). For imaging, solutions were sealed between a microscope slide and cover slip using spacers with thickness of ~150 μm. A simplified schematic for the thermal imaging set-up is shown in Fig. S1, ESI †. A 632.8 nm He-Ne laser (Meredith Instruments,) with output power of 20 mW and a 543.5 nm He-Ne laser (Melles Griot, 5mW), co-axially coupled to the same input microscope port, were used as light sources to excite the anti-Stokes and the Stokes fluorescence, correspondingly, in a probe dye (Rhodamine 640) dispersed in a sample. A Nikon inverted microscope (Eclipse TE-2000-S) with a60× NA=1.2 Nikon objective lens was employed as a base for confocal microscopy to focus the pump and probe beams onto a sample. A picosecond optical parametric oscillator (Levante Emerald, APE) pumped by Nd:YVO4 laser (picoTRAIN IC-10000/532-4000, HighQ Laser) served as a pump source at 818 nm. The pump beam with an average power of ~200 mW was coupled by a dichroic mirror into the same input microscope port, together with the 543.5 and 632.8 nm laser beams. The anti-Stokes and the reference Stokes fluorescence signals were collected in the backward direction through the microscope objective lens and directed to the PMT by the spectrally separating dichroic mirror. The notch and the barrier filters extract the anti-Stokes fluorescence signal from the laser and other radiation backgrounds. The confocal microscopy mode was realized by the use of a pinhole of diameter ~100 μm in the focal plane of the focusing lens of the PMT detection system. A computer controlled XY galvano-scanner (GSI Lumonics) together with the detection system and a custom made software interface enabled generation of optical images with a speed of 1 frame per second and with a resolution of 500×500 pixels (~4 μs per pixel acquisition speed). This experimental setup allowed in-plane (XY) scanning of the sample by the probe beam to obtain confocal imaging in the region near the stationary IR pumping beam, within the area chosen by user through the software interface between 10×10 μm^2 and 290×290 μm^2. The probe beam waist diameter was estimated to be 0.8 μm, while the pump beam waist diameter was measured to be ~2 μm. Therefore, the in-plane resolution of obtained images was close to the wavelength of scanning laser beam ~0.6 μm.

Computational details

Replica Exchange with Solute Tempering (REST) simulations: We carried out a total of four REST[22,23] simulations, one for each of *trans* MAM-CAuBP1, *cis* MAM-CAuBP1, AuBP1C-*trans* MAM and AuBP1-*cis* MAM, adsorbed at the aqueous Ag interface. All of our REST simulations modeled a single chain of the molecule adsorbed at the aqueous planar Ag(111) interface, using the Gromacs 4.5.5 software package.[24] Our recently-developed polarizable AgP-CHARMM force-field[25] was used together with the CHARMM22*[26,27] and the modified TIP3P[28] force-fields. Details of the modifications to the force-field to describe the MAM unit can be found in previous study.[29] Based on our previously published work, we used an effective temperature range spanning 300 – 433 K. A total of 17 replicas were used to span this effective temperature window over uniform intervals. All REST simulations were carried out for 25 × 10^6 MD steps, yielding conformational sampling that is approximately equivalent to μs trajectories of conventional MD.[30,31]

The initial configurations for each replica covered a range of secondary structures, including α-helix, β-turn, polyproline II and random coil conformations for the peptide component of the molecule, and either the *trans* or the *cis* configuration for the MAM component of the molecule. The adsorbate structure for each replica was initially placed so that at least one peptide atom was within ~3Å distance from the top surface of the Ag slab. The Ag(111) surface comprised a slab with a thickness of five atomic layers. All silver atoms were held fixed in position during these simulations, with only the metal atom dipoles free to rotate. Our system comprised ~6600 water molecules, and, as required, counter-ions (in the form of Na$^+$ and Cl$^-$ ions) to ensure overall charge neutrality of the simulation cell. The free (i.e. non-conjugated) peptide terminus of each molecule was modeled in zwitterionic form (i.e. either NH^{3+} or COO$^-$), consistent with the experimentally synthesized compounds. Peptide residues in each molecule were assigned a protonation state consistent with a solution pH of ~7. We used an orthorhombic periodic cell; the Ag slab had lateral dimensions 76.6 Å x 76.5 Å, with an inter-slab spacing perpendicular to the slab surface in excess of 75 Å, such that the density of liquid water in the central region between the slabs was consistent with the liquid water density at room temperature and ambient pressure. Periodic boundary conditions were applied in all three dimensions. Simulations were performed in the Canonical (NVT) ensemble, at a temperature of 300K, maintained using the Nosé-Hoover thermostat,[32-34] with a coupling constant of $\tau = 0.4$ ps. Newton's equations of motion were solved with an integration time-step of 1fs. Coordinates and velocities were saved every 1000 steps (1ps). Long-ranged electrostatic interactions were treated using Particle-mesh Ewald (PME),[35] with a cut-off at 11 Å, whereas a force-switched cut-off, starting at 9 Å and ending at 10 Å was used for Lennard-Jones non-bonded interactions.

Detailed analysis was carried out on each constant-ensemble run at an effective temperature of 300K (herein referred to as the reference trajectory). We classified the Boltzmann-weighted ensemble from our reference trajectories into groups of like structures, on the basis of similarity of their backbone structures, via the Daura clustering algorithm[36] with a root mean-squared deviation (RMSD) cutoff between backbone atoms. We defined the backbone of the molecule as the peptide backbone atoms plus the atoms along the mid-line of the MAM unit, and we applied an RMSD cutoff of 3 Å. We performed our clustering analysis over the entire 25 ns trajectory in each case. The population of a given cluster was calculated as the percentage fraction of the number of frames that were assigned membership of that cluster, divided by the total number of frames in the trajectory.

Multiscale QM/CMM calculations

From each snapshot extracted from the molecular dynamics trajectories, the model system was constructed by trimming the Ag(111) substrate to a three-layered cylinder with a cut-off radius of 15 Å, which has been shown to be sufficient for modeling the effects of metal surfaces on the optical properties of the adsorbed chromophore.[37] The range-separated CAM-B3LYP functional[38] and the def-TZVP basis set[39] were employed for the azobenzene chromophore, while the capacitance–polarization interaction model[40] was adopted for the silver substrate. The multiscale QM/CMM calculations[41] were conducted using the DALTON quantum chemistry program package.[42] For each system, the ensemble average of the calculated TPA cross-section was obtained as weighted average over the 16 most probable conformations.

The TPA transition probability is obtained from the two-state model[43]

$$\delta^{2SM} = \frac{16}{15}\frac{\left|\boldsymbol{\mu}_{0f}\right|^2 \left|\Delta\boldsymbol{\mu}\right|^2}{\Delta E^2}\left(1+2\cos^2\theta\right) \qquad (1)$$

where $\boldsymbol{\mu}_{0f}$ is the transition dipole moment, $\Delta\boldsymbol{\mu}$ is the difference between the excited and ground state dipole moments, θ is the angle between $\boldsymbol{\mu}_{0f}$ and $\Delta\boldsymbol{\mu}$, and ΔE is the excitation energy. Here $\Delta\boldsymbol{\mu}$ is computed from the double residue of the quadratic response function using the DALTON program package. The TPA cross-section is then obtained through Lorentzian convolution with a full-width-at-half-maximum Γ = 0.0037 au (0.1 eV).

$$\sigma^{2\mathrm{SM}}(\omega) = \frac{4\pi^3 \alpha a_0^5 \omega^2}{c} g(2\omega)\delta^{2\mathrm{SM}} \qquad (2)$$

$$g(2\omega) = \frac{1}{\pi}\frac{\Gamma/2}{(\Delta E - 2\omega)^2 - (\Gamma/2)^2} \qquad (3)$$

Results and discussion

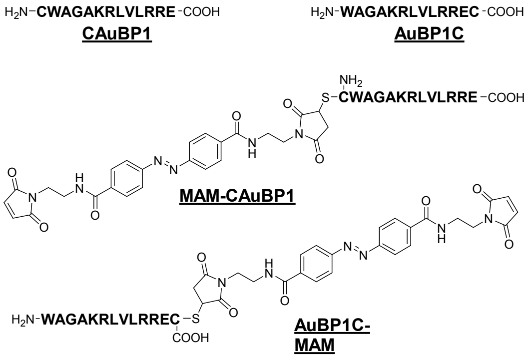

Fig. 1 Peptide sequences of CAuBP1 and AuBP1C, and chemical structures of their MAM-conjugated hybrids.

The photoswitchable maleimide-azobenzene-maleimide (MAM) molecule and its hybrids with the metal binding peptide (AuBP1C and CAuBP1) (Fig. 1) were synthesized as shown Scheme S1, ESI †.[29] For this, the carboxyl groups of azobenzene-4,4′-dicarboxylic acid were converted to acid chlorides, to facilitate nucleophilic attack on the carboxyl by N-(2-aminoethyl)-maleimide to produce the MAM. Metal binding peptides with a thiol-bearing cysteine at either the C-terminus (AuBP1C) or N-terminus (CAuBP1) were prepared and mixed with an excess of the MAM. Thiol-maleimide coupling produced the peptide/MAM hybrids (AuBP1C-MAM and MAM-CAuBP1).

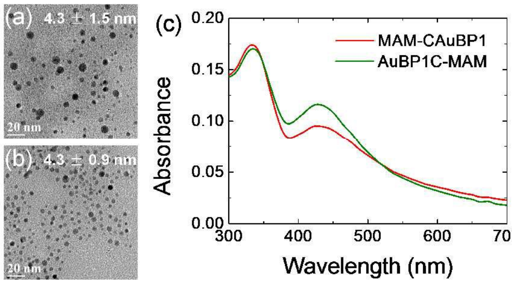

Fig. 2 TEM images of Ag nanoparticles prepared using (a) MAM-CAuBP1 and (b) AuBP1C-MAM (b) as capping agents. (c) Absorbance spectra of colloidal dispersions of the nanoparticles.

These peptide/MAM conjugates were fully characterized and then used as capping agents for growth of Ag NPs. For this, Ag^+ ions were mixed with the peptide/MAM conjugates at a 2:1 metal ion:peptide/MAM ratio, in water at room temperature. We then added $NaBH_4$, at a 3:1 ratio of $NaBH_4$ to metal ion, to generate the peptide/MAM capped Ag NPs. The products were characterized by TEM imaging and UV-vis absorbance spectroscopy (Fig. 2). TEM showed spherical particles with average diameters of 4.3 nm for Ag NPs capped with either of the hybrid molecules. The Ag NPs showed a clear LSPR absorbance band near 430 nm. All samples showed strong absorbance at 330 nm, arising mainly from the π→π* transition of the MAM. The absorbance associated with the n→π* transition, near 430 nm, was not resolvable separately from the LSPR bands. Note that the n→π* transition band overlaps almost perfectly with the LSPR band of Ag NPs (Fig. S2, ESI†). The MAM units of the hybrids on the Ag NPs were isomerized from *trans* to *cis* and *cis* to *trans* by 350 nm (π→π* transition) and 440 nm (n→π* transition) illumination, respectively (Fig. S3**,** ESI†).

To explore the possibility of LSPR enhancement of two photon induced isomerization of the azobenzene moiety, we employed femtosecond laser pulses at wavelengths of 700 and 880 nm, corresponding approximately to half the energy (double the wavelength) of the 330 nm (π→π*) transition and 430 nm (n→π*) transitions, respectively. These pulses were directed into aqueous solutions of free peptide/MAM hybrids and stable colloidal dispersions of Ag NPs capped with the peptide/MAM hybrids, for a period of 2 hours. Without D/A substitution, azobenzenes have extremely weak TPA cross-section, and thus the free peptide/MAM hybrid solutions did not show any evidence of two-photon driven isomerization at either excitation wavelength (Fig. S4**,** ESI†).

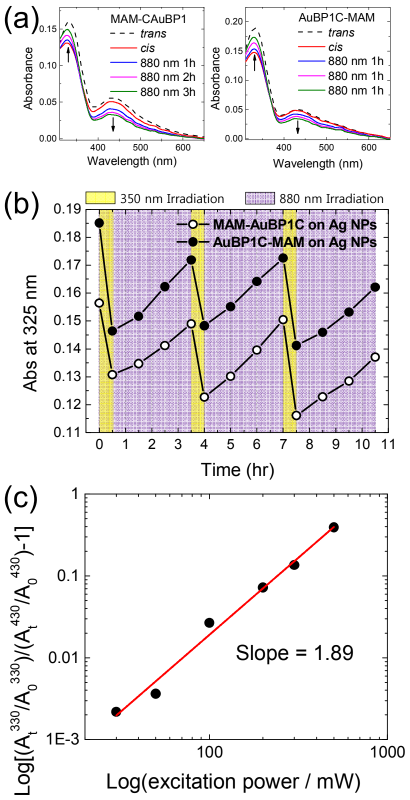

Fig. 3 (a) Time-dependent UV-vis absorbance spectra of *cis*-MAM-CAuBP1 and *cis*-AuBP1C-MAM on Ag NPs under pulsed laser illumination at 880 nm. (b) Reversibility of photo-induced switching is shown by the change in the absorbance at 330 nm under 350 nm illumination from a Xenon lamp (yellow regions) or 880 nm laser illumination (violet regions) for MAM-CAuBP1-capped Ag NPs and AuBP1C-MAM-capped Ag NPs. (c) Excitation power dependence of isomerization of *cis*-AuBP1C-MAM on Ag NPs under pulsed laser illumination at 880 nm for 1 h.

Upon 880 nm femtosecond laser illumination of Ag NPs capped with hybrid molecules in their *cis* configuration, we observed a clear increase in absorbance at 330 nm, consistent with switching of the azobenzene moiety from the *cis* to *trans* state (Fig. 3a), although this isomerization was much slower than that triggered by linear absorption. The slow switching rate can largely be attributed to the fact that the two-photon initiated process, with its nonlinear intensity dependence, occurs only at the focal spot of the laser, and thus only in a tiny fraction of the volume of the Ag NP dispersion. In contrast, the linear process, which utilizes a lamp, occurs uniformly throughout the dispersion. This highly localized response can be exploited to provide improved spatial resolution for local switching within a 3D volume. In Fig. 3a, a decrease in absorbance at 430 nm is attributable to irreversible photo-bleaching, arising from degradation or oxidation of the Ag NPs over extended periods of high-intensity pulsed laser illumination. The hybrid molecules adsorbed on the surface of Ag NPs could be repetitively switched many times by alternating single-photon and two-photon excitation, (Fig. 3b and Fig. S5, ESI†). The NPs remained stably dispersed in solution over multiple switching cycles with no evidence of aggregation.

In contrast, applying the femtosecond pulses from the 700 nm focused laser to the *trans* peptide/MAM hybrids on Ag NPs did not produce switching (Fig. S6, ESI†). Switching would produce a reduction in absorbance at 330 nm. However, the absorbance at 330 nm further decreased upon illumination at 880 nm, rather than being restored to its initial value, as it would be for reversible isomerization. This suggests that both of the decreases in absorbance result not from switching, but from a photo-bleaching process. The two-photon induced *trans* to *cis* isomerization was not facilitated by adsorption of the peptide/MAM hybrid on Ag NPs.

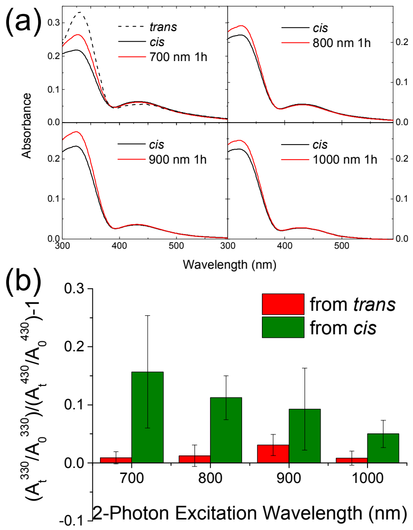

Fig. 4 Observation of excitation wavelength dependence of two-photon switching of MAM-CAuBP1 capped Ag NPs. (a) Changes in absorbance spectra of *cis*-MAM-CAuBP1 capped Ag NPs upon 700 ~ 1000 nm laser illumination for 1 h. (b) Graph representing two-photon-induced *trans* to *cis* (red) and *cis* to *trans* (green) switching behaviors upon the laser excitation.

To confirm the nonlinear optical character of the NIR laser induced *cis* to *trans* isomerization, we measured the isomerization behavior of *cis*-AuBP1C-MAM on Ag NPs under 880 nm laser illumination as a function of the excitation power. A two-photon process should show quadratic dependence upon illumination intensity. Because any decrease of the broad absorption band at 430 nm due to photobleaching should also produce a decrease of the 330 nm absorbance, we divided the relative absorbance at 330 nm ($A_{330}/A_{330,0}$) by the relative absorbance at 430 nm ($A_{430}/A_{430,0}$), where $A_{330,0}$ and $A_{430,0}$ are the absorbances before illumination, and A_{330} and A_{430} are the absorbances after illumination. We plotted this as $(A_{330}/A_{330,0})/(A_{430}/A_{430,0}) - 1$ in Fig. S7, ESI†. Up to 50 mW pump power, no significant isomerization was observed. However, for illumination intensities of 100 mW or higher, the isomerization increased nonlinearly with increasing laser power. When plotted on a log-log scale the power dependence was fit well by a line with slope 1.89 ± 0.1 (Fig. 3c), consistent with a two-photon process.[44,45]

To explore the wavelength dependence of the two-photon driven isomerization, we illuminated *trans* and *cis* isomers of MAM-CAuBP1 on Ag NPs at wavelengths from 700 to 1000 nm. Interestingly, the spectroscopic results for the *cis* isomer indicated that two photon-induced isomerization occurred for all wavelengths, even though some of them are closer to double the wavelength of the $\pi \rightarrow \pi^*$ transition than to that of the $n \rightarrow \pi^*$ transition (Fig. 4). When the *trans* isomer was illuminated at these wavelengths, both the 330 and 430 nm absorbance decreased simultaneously (Fig. S8, ESI†) due to photobleaching. For *trans* to *cis* isomerization, A_{330} should decrease while A_{430} increases, producing a negative value of this measure of relative absorbance. However, illumination of the *trans* isomer gave small positive values of this quantity, showing that photobleaching is the main reason for the decrease in A_{330} in this case. On the other hand, illumination of the *cis* isomer with femtosecond pulses at these wavelengths gave much larger positive values, reflecting the *cis* to *trans* isomerization that occurs in this case.

The observed two-photon initiated *cis* to *trans* isomerization can be explained by selective activation of TPA in the *cis* MAM occurring at its interface with the Ag NPs. Typically, excitations at the $\pi \rightarrow \pi^*$ and at the $n \rightarrow \pi^*$ transition energies of azobenzene have been applied for *cis* to *trans* and *trans* to *cis* isomerization, respectively. However, prior studies have shown that each transition does not initiate isomerization in only one direction (Fig. S9a, ESI†).[46] Rather, each transition contributes to both isomerization directions, even though the degree of their contributions is different. The significant difference between single photon and two-photon isomerization is that the TPA cross-section of the *trans* MAM is not enhanced by the LSPR of Ag NPs. Thus, the *trans* isomer on Ag NPs cannot isomerize back to the *cis* isomer even if the *trans*- to *cis*- isomerization is favored by the laser wavelength. This shifts the population at the photo-stationary state towards the *trans* isomer for all of the TPE wavelengths (Fig. S9b, ESI†).

Because the *trans* isomer is thermodynamically favored over the *cis* isomer, the *cis* to *trans* isomerization can also be activated by local heating. To determine whether local heating could be contributing to the observed behavior, we mapped the thermal profile of MAM-CAuBP1 capped Ag NPs upon TPE. To estimate the local thermal loading introduced by the Ag NPs upon excitation by near-IR laser, we employed confocal anti-Stokes fluorescence imaging using Rhodamine 101 dye as an anti-Stokes probe.[47,48] For comparison we also imaged the local thermal gradient produced by absorption of the same IR laser beam in a solution of tris[4-(7-benzothiazol-2-yl-9,9-diethylfluoren-2-yl)phenyl]amine two-photon dye (AF-350), whose fluorescence quantum yield is low, which means that the absorbed energy is primarily dissipated via non-radiative channels. According to the thermal imaging results, obtained for solutions of Ag NPs and two-photon dye samples, the latter produced a clearly visible temperature gradient under local excitation by near-IR laser illumination (Fig. S10a and black curve in Fig. S10c, ESI†). Illumination of the MAM-CAuBP1 capped Ag NPs did not produce any temperature gradient under the same conditions of local IR excitation, at least at the level of our instrument sensitivity of ~0.2 °C (Fig. S10b and red curve in Fig. S10c, ESI†). As a result, the contribution of a photothermal effect to the plasmon induced two-photon isomerization can be ruled out.

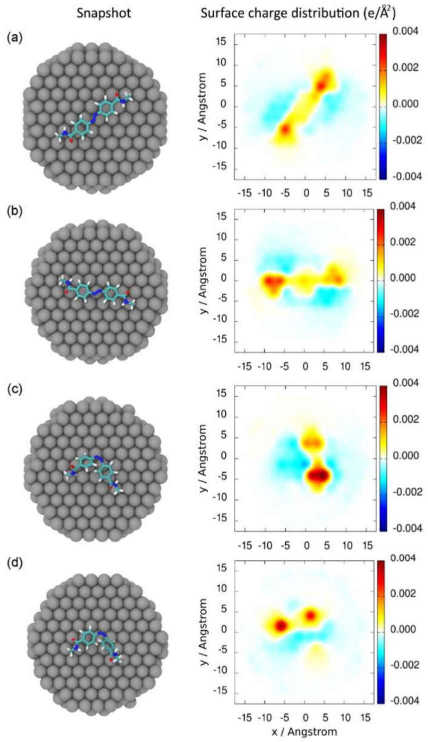

Fig. 5 Snapshot of azobenzene on the Ag(111) surface and charge distribution on the metal surface. (a) *trans*-Azobenzene conjugated to the C-terminus; (b) *trans*-azobenzene conjugated to the N-terminus; (c) *cis*-azobenzene conjugated to the C-terminus; (d) *cis*-azobenzene conjugated to the N-terminus.

Quantum chemical calculations, in partnership with state-of-the-art advanced molecular simulations, provide further insight into the working mechanism of the two-photon initiated azobenzene isomerization. In this approach, the structural inputs for our multiscale Quantum Mechanics/Capacitance Molecular Mechanics (QM/CMM) calculations were based on the conformational ensemble predicted by our Replica Exchange with Solute Tempering (REST) simulations[22,23] of the Ag-adsorbed molecules. These simulations provided a set of the most likely adsorbed conformations and the probability of their appearance in the conformational ensemble. These probabilities were then used to generate a weighted average of the calculated TPA cross-section. The frontier molecular orbitals of *trans* and *cis* azobenzene are shown in Fig. S11, ESI†. Time-dependent density functional theory (TD-DFT) calculations show that the lowest excited state S_1 of *trans*-azobenzene corresponds to the HOMO−1 → LUMO transition with $n\rightarrow\pi^*$ character, and that the S_2 state is correlated with a HOMO → LUMO transition which is of $\pi\rightarrow\pi^*$ character. For the S_1 state, the ensemble average of TPA cross-section of the *trans*-azobenzene chromophore is rather small (around 0.01 GM, see Table S1, ESI†), with excitation energy of around 0.97 eV. The inclusion of the Ag(111) surface in our multiscale QM/CMM calculations showed negligible effects on both the photon energies and the TPA cross-sections. The TPA cross-section of the S_2 state of the *trans*-azobenzene chromophore is of larger magnitude (1.76 and 1.25 GM for C- and N-terminus conjugation, respectively), and the Ag(111) surface leads to a slight alternation of the TPA cross-section (-8% and +16% for C- and N-terminus conjugation, respectively). It is interesting to observe that the *trans*-azobenzene conjugated to the N-terminus shows an opposite trend compared with that conjugated to the C-terminus, which arises from geometry relaxation of *trans*-azobenzene in different environments.

The lowest excited state S_1 of *cis*-azobenzene (HOMO → LUMO) corresponds to $n\rightarrow\pi^*$ excitation, while higher excited states such as S_2 (HOMO−4 → LUMO) and S_3 (HOMO−1 → LUMO) are $\pi\rightarrow\pi^*$ transitions with very close excitation energies (Fig. S11, ESI†). The ensemble average of the TPA cross-section of the S_1 state is 0.11 GM for the *cis*-azobenzene in vacuum (Table S2, ESI†). The TPA cross-sections for S_2 and S_3 states reach much larger values, ranging from 1 to 3 GM. Notably, the Ag(111) surface brings about a much larger enhancement of the TPA cross-section compared with that for *trans*-azobenzene. In particular, the enhancement results in TPA cross-section of 3.78 GM for the S_2 state of the C-terminus-conjugated *cis*-azobenzene, which constitutes a 129% increase. The largest absolute value of the TPA cross-section for *cis*-azobenzene adsorbed on Ag(111) surface is almost two-fold that of *trans*-azobenzene.

The different effects of metal surfaces on TPA cross-sections of *trans*- and *cis*-azobenzene could be explained by the surface charge distribution of the silver surface, as shown in Fig. 5. In both *trans*- and *cis*-azobenzene, the transition dipole moments of the $S_0\rightarrow S_1$ and $S_0\rightarrow S_2$ excitations are approximately aligned along the line connecting the two phenyl rings. When *trans*-azobenzene is physisorbed onto Ag(111) surface, the electron-rich carbonyl, phenyl and azo groups induce a large area of positive image charges beneath the azobenzene molecule, leading to a charge gradient that is almost perpendicular to the transition dipole moment of the chromophore. Thus the Ag(111) surface produces negligible effects on the optical excitation process of *trans*-azobenzene. In contrast, only one phenyl ring of *cis*-azobenzene is physisorbed onto the Ag(111) surface to generate strongly positive image charges, with the other phenyl ring being forced to tilt away from the surface. The tilted phenyl ring interacts only weakly with the surface, and the positive charges are then accumulated underneath. This results in a charge gradient that is almost parallel with the transition dipole moment of the *cis*-azobenzene molecules, thus enhancing its two-photon transition amplitude, in particular the xx component.

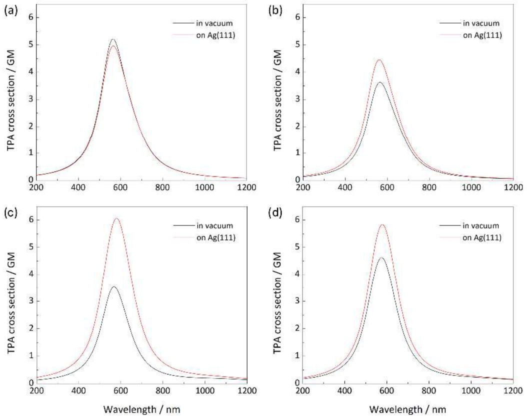

Fig. 6 Computed two-photon absorbance of azobenzene in vacuum and on Ag(111) surface. (a) *trans*-Azobenzene conjugated to the C-terminus; (b) *trans*-azobenzene conjugated to the N-terminus; (c) *cis*-azobenzene conjugated to the C-terminus; (d) *cis*-azobenzene conjugated to the N-terminus.

Theoretical modeling suggests that the Ag(111) surface is able to notably enhance the TPA cross-section of *cis*-azobenzene, while such effect for *trans*-azobenzene is much less pronounced (Fig. 6). In these calculations, the use of the two-state-model is motivated by the fact that calculations using quadratic response theory or a sum-over-states approach often encounter numerical instability due to coincidence between the energy of the incoming photon for higher excited states and the excitation energy of lower excited states. We verified the applicability of the two-state-model by examining the dipole moments and transition dipole moments, as listed in Tables S3 and S4. The significant contributions, including $\langle 0|\mu|0\rangle$, $\langle 0|\mu|2\rangle$ and $\langle 2|\mu|2\rangle$, are taken into account by the two-state-model for the second excited state. The transition dipole moment between the first and the second excited state, $\langle 1|\mu|2\rangle$, is of rather small magnitude, particularly for the case of trans-azobenzene. Moreover, the effect of Ag(111) on $\langle 0|\mu|2\rangle$ of trans-azobenzene is insignificant, consistent with the weak enhancement of TPA. The calculated individual TPA cross-sections for each conformation are shown in Tables S5 and S6. The enhancement effect on the TPA cross-section by silver substrate arises from the collective behavior of the electrons of the metal atoms, which are able to migrate almost freely within the metal region and thereby introduce the image charge effect on the adsorbed molecule. As an illustration of such effects, we show the local electric field enhancement for Ag NPs placed in a uniform external electric field (Fig. S12, ESI†). The spatial distribution of the electric field is averaged over random orientations of the external electric field. As can be seen from the cross-sectional view of the distribution of the electric field strength, the local field is considerably enhanced at the surface of the Ag NPs. Our study thus shows that charge transfer and charge polarization within a metallic cluster can substantially modify TPA absorption of certain structures of cluster physisorbed molecules. The present implementation of our QM/CMM theory using real atomic polarizabilities (in addition to capacitances) in the metallic part does not include the generation of plasmons within the cluster per se. However, it is clear that the degree of charge migration and charge imaging within a cluster has a relation to the magnitude of free carrier density upon which classical plasmon models are commonly based (jellium model), and thus that a charge imaging effect on a property in this sense has a bearing on a concomitant plasmon induced effect. Current work on implementing atomic complex polarizabilities in addition to capacitances in the QM/CMM model will indeed include (atomically resolved) plasmon effects in the theory, which will probably make the connection between the effects of charge imaging and plasmon generation on molecular properties more direct.[30]

Conclusions

In summary, we have introduced the concept of LSPR-assisted two-photon induced isomerization for a non D/A modified azobenzene moiety by non-covalent coupling with metal nanoparticles. Notably, the *cis* isomer of a symmetric amide modified azobenzene (MAM) non-covalently bound on Ag NPs was repetitively isomerized from its *cis* to *trans* configuration by TPE. This LSPR enhancement selectively promoted the *cis* to *trans* isomerization, but not the *trans* to *cis* isomerization, driving unidirectional isomerization from cis to trans under excitation at wavelengths from 700 to 1000 nm. Confocal anti-Stokes fluorescence imaging showed that this nonlinear behavior was not due to local heating, strongly suggesting that this phenomenon is electronic in origin. Through an integrated modeling approach, combining advanced conformational sampling with Quantum Mechanics/Capacitance Molecular Mechanics and response theory, we showed that charge transfer and image charges in the metallic cluster generate local fields that enhance TPA of the *cis* isomer. Additionally, the *cis* to *trans* isomerization can be promoted by the field enhancement at frequencies in the LSPR band of the Ag NPs, which overlaps with the n-π* band of the azobenzene moiety. This highly localized two-photon initiated switching could be of great practical value, as it may allow targeted switching near the focal point of an illuminating laser within the interior of a 3D assembly to modulate chemical and physical properties at desired positions.

Acknowledgements

This material is based upon work supported by the Air Force Office of Scientific Research, grant number FA9550-12-1-0226. We gratefully acknowledge the Victorian Life Sciences Computation Facility (VLSCI) for allocation of computational resources, and TRW thanks veski for an Innovation Fellowship.

References

1 R. Pardo, M. Zayat and D. Levy, *Chem. Soc. Rev.* 2011, **40**, 672.
2 Y. Yan, J. I. L. Chen and D. S. Ginger, *Nano Lett.* 2012, **12**, 2530.
3 A. S. Kumar, T. Ye, T. Takami, B. C. Yu, A. K. Flatt, J. M. Tour and P. S. Weiss, *Nano Lett.* 2008, **8**, 1644.
4 A. Manna, P.-L. Chen, H. Akiyama, T.-X. Wei, K. Tamada and W. Knoll, *Chem. Mater.* 2003, **15**, 20.
5 H. M. Bandara and S. C. Burdette, *Chem. Soc. Rev.* 2012, **41**, 1809.
6 M. Irie, *Chem. Rev.* 2000, **100**, 1685.
7 G. Berkovic, V. Krongauz and V. Weiss, *Chem. Rev.* 2000, **100**, 1741.
8 S. Kawata and Y. Kawata, *Chem. Rev.* 2000, **100**, 1777.
9 D. Bleger, Z. Yu and S. Hecht, *Chem. Commun.* 2011, **47**, 12260.
10 S. Kobatake, S. Takami, H. Muto, T. Ishikawa and M. Irie, *Nature* 2007, **446**, 778.
11 A. S. Dvornikov, E. P. Walker and P. M. Rentzepis, *J. Phys. Chem. A* 2009, **113**, 13633.
12 L. Antonov, K. Kamada, K. Ohta and F. S. Kamounah, *Phys. Chem. Chem. Phys.* 2003, **5**, 1193.
13 M. Izquierdo-Serra, M. Gascón-Moya, J. J. Hirtz, S. Pittolo, K. E. Poskanzer, È. Ferrer, R. Alibés, F. Busqué, R. Yuste, J. Hernando and P. Gorostiza, *J. Am. Chem. Soc*. 2014, **136**, 8693.
14 D.-L. Jiang and T. Aida, *Nature* 1997, **388**, 454.
15 Y. Tsuboi, R. Shimizu, T. Shoji and N. Kitamura, *J. Am. Chem. Soc.* 2009, **131**, 12623.
16 I. Cohanoschi and F. E. Hernandez, *J. Phys. Chem. B.* 2005, **109**, 14506.
17 S. T. Sivapalan, J. H. Vella, T. K. Yang, M. J. Dalton, J. E. Haley, T. M. Cooper, A. M. Urbas, L. S. Tan and C. J. Murphy, *J. Phys. Chem. Lett.* 2013, **4**, 749.
18 W. Wenseleers, F. Stellacci, T. Meyer-Friedrichsen, T. Mangel, C. A. Bauer, S. J. K. Pond, S. R. Marder and J. W. Perry, *J. Phys. Chem. B* 2002, **106**, 6853.
19 A. Campion and P. Kambhampati, *Chem. Soc. Rev.* 1998, **27**, 241.
20 E. Fort and S. Grésillon, *J. Phys. D: Appl. Phys.* 2008, **41**, 013001.
21 M. Hnilova, E. E. Oren, U. O. Seker, B. R. Wilson, S. Collino, J. S. Evans, C. Tamerler and M. Sarikaya, *Langmuir* 2008, **24**, 12440.
22 T. Terakawa, T. Kameda and S. Takada*, J. Comput. Chem.* 2011, **32**, 1228.
23 L. B. Wright and T. R. Walsh, *Phys. Chem. Chem. Phys.* 2013, **15**, 4715.
24 B. Hess, C. Kutzner, D. van der Spoel and E. Lindahl, *J. Chem. Theory Comput.* 2008, **4**, 435.
25 Z. E. Hughes, L. B. Wright and T. R. Walsh, *Langmuir* 2013, **29**, 13217.
26 A. D. MacKerell, D. Bashford, M. Bellott, R. Dunbrack, J. D. Evanseck, M. J. Field, S. Fischer, J. Gao, H. Guo and S. Ha, *J. Phys. Chem. B* 1998, **102**, 3586.
27 S. Piana, K. Lindorff-Larsen and D. E. Shaw, *Biophys. J.* 2011, **100**, L47.

28 W. L. Jorgensen, J. Chandrasekhar, J. D. Madura, R. W. Impey and M. L. Klein, *J. Chem. Phys.* 1983, **79**, 926.

29 Z. Tang, C.-K. Lim, J. P. Palafox-Hernandez, K. L. M. Drew, Y. Li, M. T. Swihart, P. N. Prasad, T. R. Walsh and M. R. Knecht, *Nanoscale* 2015, **7**, 13638.

30 X. Li, Z. Rinkevicius and H. Ågren, *J. Chem. Theory Comput*. 2014, **10**, 435.

31 Z. Tang, J. P. Palafox-Hernandez, W. C. Law, Z. E. Hughes, M. T. Swihart, P. N. Prasad, M. R. Knecht and T. R. Walsh, *ACS Nano* 2013, **7**, 9632.

32 S. Nosé, *Mol. Phys.* 1984, **52**, 255.

33 S. Nosé, *J. Chem. Phys.* 1984, **81**, 511.

34 W. G. Hoover, *Phys. Rev. A* 1985, **31**, 1695.

35 T. Darden, D. York and L. Pedersen, *J. Chem. Phys.* 1993, **98**, 10089.

36 X. Daura, K. Gademann, B. Jaun, D. Seebach, W. F. van Gunsteren and A. E. Mark, *Angew. Chem. Int. Ed.* 1999, **38**, 236.

37 Z. Rinkevicius, X. Li, J. A. Sandberg, K. V. Mikkelsen and H. Ågren, *J. Chem. Theory Comput.* 2014, **10**, 989.

38 T. Yanai, D. P. Tew and N. C. Handy, *Chem. Phys. Lett.* 2004, **393**, 51.

39 A. Schäfer, C. Huber and R. Ahlrichs, *J. Chem. Phys.* 1994, **100**, 5829.

40 S. M. Morton and L. Jensen, J. Chem. Phys. 2010, **133**, 074103.

41 Z. Rinkevicius, X. Li, J. A. Sandberg and H. Ågren, *Phys. Chem. Chem. Phys.* 2014, **16**, 8981.

42 K. Aidas, C. Angeli, K. L. Bak, V. Bakken, R. Bast, L. Boman, O. Christiansen, R. Cimiraglia, S. Coriani, P. Dahle, E. K. Dalskov, U. Ekström, T. Enevoldsen, J. J. Eriksen, P. Ettenhuber, B. Fernández, L. Ferrighi, H. Fliegl, L. Frediani, K. Hald, A. Halkier, C. Hättig, H. Heiberg, T. Helgaker, A. C. Hennum, H. Hettema, E. Hjertenæs, S. Høst, I.-M. Høyvik, M. F. Iozzi, B. Jansik, H. J. Aa. Jensen, D. Jonsson, P. Jørgensen, J. Kauczor, S. Kirpekar, T. Kjærgaard, W. Klopper, S. Knecht, R. Kobayashi, H. Koch, J. Kongsted, A. Krapp, K. Kristensen, A. Ligabue, O. B. Lutnæs, J. I. Melo, K. V. Mikkelsen, R. H. Myhre, C. Neiss, C. B. Nielsen, P. Norman, J. Olsen, J. M. H. Olsen, A. Osted, M. J. Packer, F. Pawlowski, T. B. Pedersen, P. F. Provasi, S. Reine, Z. Rinkevicius, T. A. Ruden, K. Ruud, V. Rybkin, P. Salek, C. C. M. Samson, A. Sánchez de Merás, T. Saue, S. P. A. Sauer, B. Schimmelpfennig, K. Sneskov, A. H. Steindal, K. O. Sylvester-Hvid, P. R. Taylor, A. M. Teale, E. I. Tellgren, D. P. Tew, A. J. Thorvaldsen, L. Thøgersen, O. Vahtras, M. A. Watson, D. J. D. Wilson, M. Ziolkowski and H. Ågren. *WIREs Comput. Mol. Sci.* 2014, **4**, 269.

43 P. Cronstrand, Y. Luo and H. Ågren, *Chem. Phys. Lett.* 2002, **352**, 262.

44 W. Denk, J. H. Strickler and W. W. Webb, *Science* 1990, **248**, 73.

45 D. R. Larson, W. R. Zipfel, R. M. Williams, S.W. Clark, M. P. Bruchez, f. W. Wise and W. W. Webb, Science 2003, **300**, 1434.

46 C. R. Crecca and A. E. Roitberg, *J. Phys. Chem. A* 2006, **110**, 8188.

47 A. V. Kachynski, A. N. Kuzmin, H. E. Pudavar and P. N. Prasad, *Appl. Phys. Lett.* 2005, **87**, 023901.

48 A. N. Kuzmin, A. Baev, A.V. Kachynski, T. S. Fisher, A. Shakouri and P. N. Prasad, *J. Appl. Phys.* 2011, **110**, 033512.

Graphical Abstract

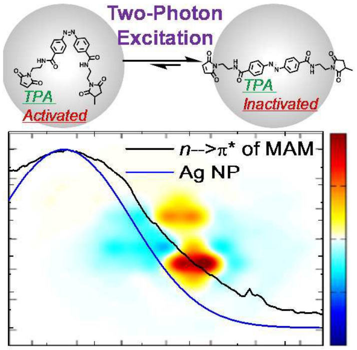

Enhanced two-photon absorption through charge and plasmon interactions between Ag NPs and a non-donor/acceptor modified azobenzene allow selective two-photon initiated *cis* to *trans* isomerization.